Ultrasound in Med. & Biol., Vol. 39, No. 9, pp. 1688–1697, 2013

0301-5629/$ - see front matter

http://dx.doi.org/10.1016/j.ultrasmedbio.2013.02.463

● *Original Contribution*

ELASTIC IMAGE REGISTRATION TO QUANTIFY 3-D REGIONAL MYOCARDIAL DEFORMATION FROM VOLUMETRIC ULTRASOUND: EXPERIMENTAL VALIDATION IN AN ANIMAL MODEL

Brecht Heyde,* Stefaan Bouchez,† Sabine Thieren,* Michael Vandenheuvel,† Ruta Jasaityte,* Daniel Barbosa,* Piet Claus,* Frederik Maes,‡ Patrick Wouters,† and Jan D'hooge*§

*Laboratory on Cardiovascular Imaging and Dynamics, KU Leuven, Leuven, Belgium; †Department of Anesthesiology, Ghent University, Ghent, Belgium; ‡Medical Image Computing (ESAT/PSI), KU Leuven, Leuven, Belgium; and §Medical Imaging Lab, Norwegian Institute for Science and Technology, Trondheim, Norway

(*Received* 9 *January* 2013; *revised* 19 *February* 2013; *in final form* 24 *February* 2013)

Abstract—Although real-time 3-D echocardiography has the potential to allow more accurate assessment of global and regional ventricular dynamics compared with more traditional 2-D ultrasound examinations, it still requires rigorous testing and validation should it break through as a standard examination in routine clinical practice. However, only a limited number of studies have validated 3-D strain algorithms in an *in vivo* experimental setting. The aim of the present study, therefore, was to validate a registration-based strain estimation methodology in an animal model. Volumetric images were acquired in 14 open-chest sheep instrumented with ultrasonic microcrystals. Radial strain (ε_{RR}), longitudinal strain (ε_{LL}) and circumferential strain (ε_{CC}) were estimated during different stages: at rest, during reduced and increased cardiac inotropy induced by esmolol and dobutamine infusion, respectively, and during acute ischemia. Agreement between image-based and microcrystal-based strain estimates was evaluated by their linear correlation, indicating that all strain components could be estimated with acceptable accuracy ($r = 0.69$ for ε_{RR}, $r = 0.64$ for ε_{LL} and $r = 0.62$ for ε_{CC}). These findings are comparable to the performance of the current state-of-the-art commercial 3-D speckle tracking methods. Furthermore, shape of the strain curves, timing of peak values and location of dysfunctional regions were identified well. Whether 3-D elastic registration performs better than 3-D block matching-based methodologies still remains to be proven. (E-mail: brecht.heyde@med.kuleuven.be) © **2013 World Federation for Ultrasound in Medicine & Biology.**

Key Words: **Echocardiography, Elastic registration, Sonomicrometry, Strain, Validation, In vivo.**

INTRODUCTION

In daily clinical practice, echocardiography is a well established, non-invasive and attractive imaging modality for the evaluation of cardiac function and mechanics. Myocardial deformation imaging is used widely to facilitate detection of cardiac pathologies such as acute ischemia (Kukulski et al. 2003) and coronary artery disease (Bijnens et al. 2007), monitor disease progression, provide disease prognosis or quantify left ventricular (LV) dyssynchrony (Mor-Avi et al. 2011).

Although real-time 3-D echocardiography (RT3DE) has been available for several years, ongoing advances in both transducer hardware and ultrasound (US) computer software have sparked research interest, not only academically but also commercially, as most major vendors of clinical echocardiographic imaging systems currently offer RT3DE solutions. The advent of this 3-D strain era holds promise as it potentially allows for a faster and more accurate assessment of global and regional ventricular dynamics, while overcoming the intrinsic limitations associated with 2-D strain estimation such as out-of-plane motion.

Various methods have been developed to estimate motion and deformation from volumetric ultrasound sequences. According to the classification proposed in Jasaityte et al. (2013), they can roughly be subdivided into three categories, all differing in their underlying tracking algorithm. First, block matching-based methods have received widespread attention in the ultrasound community and have successfully been applied to volumetric images (Crosby et al. 2009; Duan et al. 2009; Lopata et al. 2011). They share the same underlying

Address correspondence to: Brecht Heyde, Herestraat 49, bus 7003, 3000 Leuven, Belgium. E-mail: brecht.heyde@med.kuleuven.be

principle with the more general optical flow-based formulation: motion is characterized by a flow of pixels with an assumed constant intensity. Second, elastic or non-rigid image registration techniques, popular in the image processing society, have also been proposed to quantify myocardial motion (De Craene et al. 2012b; Elen et al. 2008; Heyde et al. 2012; Myronenko et al. 2009). They employ image warping techniques to estimate cardiac motion between subsequent frames. The myocardial deformation field is typically parametrized using smooth basis functions, for example, B-splines (Kybic and Unser 2003). Because not all warping solutions are feasible or desirable, additional conditions are usually imposed (*e.g.,* tissue motion is smooth in space and/or time) to regularize the obtained deformation field. Finally, model-based approaches incorporate a priori knowledge into the motion estimation process, for example, a biomechanical model describing the presence of myocardial fibers (Papademetris et al. 2001) or a statistical model capturing the LV appearance in a large annotated database (Leung et al. 2011). Within each category several commercial implementations exist (*e.g.,* Reant et al. 2012; Seo et al. 2009; Somphone et al. 2008; Yang et al. 2011).

Although all these 3-D strain estimation methods measure the same deformation of the heart, they do it in different ways, for example, by using different regularization choices or postprocessing steps (Marwick 2012). This was demonstrated in a recent study by Gayat et al. (2011), who reported a high intervendor dependency of strain measures. Therefore, it is essential that every method is validated individually before being introduced into clinical practice.

In this work we focus on a registration-based methodology. We have previously reported that this technique is reliable in extracting *global* LV functional parameters in simulated ultrasound (US) data sets (Elen et al. 2008). Recently, the encouraging performance of this approach was further illustrated on volumetric data obtained from tissue-mimicking phantoms on a *regional* level (Heyde et al. 2012) and was shown to outperform block matching-based methods in an animal setting for 2-D image data (Heyde et al. 2013).

The aim of the present study was to further validate this methodology in volumetric images of an animal model by comparing the estimated strain values with a known ground truth, obtained through sonomicrometry.

METHODS

Animal preparation

Fourteen female Suffolk sheep (44.3 ± 10.4 kg) were premedicated with an intragluteal injection of ketamine (10 mg/kg) and piritramide (1 mg/kg). Anesthesia was induced via a cephalic vein with an intravenous infusion of propofol (10 mg/kg) and a bolus of sufentanil (0.5 μg/kg). The sheep were mechanically ventilated throughout the procedure with a mixture of sevoflurane, oxygen and room air to maintain normocapnia and normoxia (tidal volume of 8 mL/kg and respiratory rate of 12/min). Anesthesia was maintained with a continuous infusion of sufentanil (1 μg/kg/h) and an end-tidal sevoflurane concentration of 2.5%.

A bilumen catheter was inserted into the left jugular vein to allow measurement of the central venous pressure and administration of drugs. Furthermore, a catheter-tipped pressure transducer (Millar, Houston, TX, USA) was advanced into the left ventricle via the right carotid artery for the continuous monitoring of LV pressure and its first temporal derivative (dP/dt). The systemic arterial pressure and heart rate were measured in the proximal aorta via a fluid-filled side arm of the arterial sheath.

A sternotomy was performed, and the heart was suspended in a pericardial cradle to maintain a normal anatomic configuration. Cardiac output was monitored with a flow probe positioned around the pulmonary artery.

In all animals, reference radial (ε_{RR}), longitudinal (ε_{LL}) and circumferential (ε_{CC}) strain components were obtained using four ultrasonic microcrystals (2 mm in diameter, Sonometrics Corp, London, ON, Canada) attached to the myocardium in the mid-inferolateral wall in a tetrahedral configuration (see Fig. 1). Three crystals were sutured directly to the epicardium, resulting in two crystal pairs along the circumferential and longitudinal directions, respectively, whereas a fourth crystal was placed subendocardially just radially to the center crystal. The latter was introduced in an oblique way to limit damage to the myocardium under investigation.

This investigation conforms to the Public Health Service Policy on Humane Care and Use of Laboratory Animals published by the Office of Laboratory Animal Welfare of the U.S. National Institutes of Health (revised 2008) and was approved by the local ethics committee (Ethische Commissie Dierproeven, Ghent University, Ghent, Belgium).

Data acquisition

A GE Vivid7 ultrasound scanner (GE Vingmed, Horten, Norway) equipped with a 2-D matrix transducer (3V probe) was used to acquire volumetric data at a frame rate of 25–32 Hz with elecrocardiographic gating over four cardiac cycles. The left ventricle was scanned from an apical position using a liver as a stand-off. The optimal combination of spatial and temporal resolution was achieved by decreasing the volume size and depth to the smallest setting possible, while keeping the whole left ventricle within the field of view.

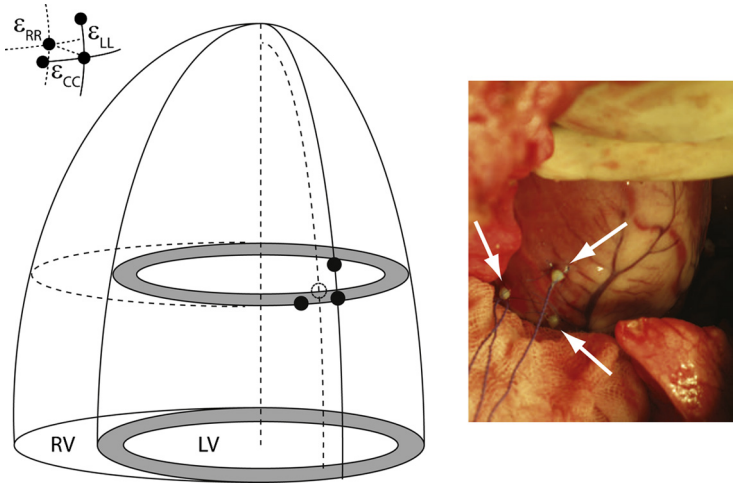

Fig. 1. Four sonomicrometry crystals were sutured into the infero-lateral wall of the myocardium in a tetrahedral configuration to obtain ground-truth myocardial deformation for the radial (ε_{RR}), longitudinal (ε_{LL}) and circumferential (ε_{CC}) strain components.

After the image data were collected at rest, the range of strain values was modulated by reducing the inotropy with esmolol infusion and, subsequently, by increasing it with dobutamine administration. A physiological target was set as a 50% reduction in $(dP/dt)_{max}$ and a 100% increase in $(dP/dt)_{max}$ relative to baseline for esmolol and dobutamine respectively. Infusion rates were titrated continuously according to this target. In the final stage, acute ischemia was induced by ligating a distal branch of the circumflex coronary artery. Ischemia measurements could not be completed in three animals, and esmolol data were lacking in two others. Two data sets had to be excluded from the analysis because of image dropout artifacts in the inferolateral region. Overall, 49 data sets could thus be included for further analysis.

Because of the overlapping frequency bands of the microcrystals and the ultrasound system, both systems could not be operated simultaneously. Therefore, crystal data were acquired immediately before and after each stage, and the system was switched off during ultrasound recordings.

Elastic image registration

The acquired images were processed using an elastic image registration approach previously developed in our laboratory (Elen et al. 2008; Heyde et al. 2012). During registration, one image associated with frame $f + 1$ (*i.e.*, the floating image $\mathbf{I}_{f+1}$) is warped to another image associated with frame f (*i.e.,* the reference image $\mathbf{I}_f$). The goal of this process is to find a displacement field $\mathbf{u}_{f\to f+1}(\mathbf{r})$ in each point $\mathbf{r} = [x, y, z]$ that makes $\mathbf{I}_{f+1}(\mathbf{r} + \mathbf{u}_{f\to f+1}(\mathbf{r}))$ spatially aligned with $\mathbf{I}_f(\mathbf{r})$ (Zitova and Flusser 2003).

In the present work, inter-frame myocardial displacement was modeled with a 3-D third-order B-spline tensor product (Kybic and Unser 2003):

$$\mathrm{u}_{f\to f+1}(\mathbf{r}) = \sum_{i\in N_i}\sum_{j\in N_j}\sum_{k\in N_k}\mu_{ijk}\beta_x\left(\frac{x-\lambda_i}{\sigma_x}\right)\beta_y\left(\frac{y-\lambda_j}{\sigma_y}\right)\beta_z\left(\frac{z-\lambda_k}{\sigma_z}\right) \quad (1)$$

with $[\lambda_i, \lambda_j, \lambda_k]$ and $[\sigma_x, \sigma_y, \sigma_z]$ the control point location and spacing in the $[x, y, z]$ direction, respectively. N_i, N_j and N_k are the set of control points within the compact support of the B-spline β_x, β_y and β_z, respectively.

As image intensities at corresponding points between two consecutive frames are similar for intra-modality registration, the sum-of-squared differences was used as an image similarity metric. The optimal transformation field $\mathbf{T}_{f\to f+1}(\mathbf{r}) = \mathbf{r}+\mathbf{u}_{f\to f+1}(\mathbf{r})$ was estimated iteratively with a limited-memory Broyden Fletcher Goldfarb Shannon optimization routine with simple bounds (LBFGSB [Byrd et al. 1995]), as this optimizer was found to perform well for optimization of a large amount of parameters while also eliminating the need for storing the inverse of the Hessian matrix during the optimization routine. To capture small deformations, the model complexity was gradually increased in three stages by refining the B-spline grid with a factor of 2 in every stage. Regularization was performed during the optimization process by the addition of a smoothness penalty based on the 3-D equivalent of the bending energy of a 2-D thin sheet of metal (Rueckert et al. 1999) in the cost function E:

$$E = \frac{1}{n}\sum_{\mathbf{r}\in\mathbf{I}_f}\left[\mathbf{I}_f(\mathbf{r}) - \mathbf{I}_{f+1}(\mathbf{T}(\mathbf{r}))\right]^2 + \frac{\alpha}{n}\sum_{\mathbf{r}\in\mathbf{I}_f}\left\|\frac{\partial^2\mathbf{T}(\mathbf{r})}{\partial\mathbf{r}\partial\mathbf{r}^T}\right\|_F^2 \quad (2)$$

where

$$\begin{aligned}\left\|\frac{\partial^2\mathbf{T}(\mathbf{r})}{\partial\mathbf{r}\partial\mathbf{r}^T}\right\|_F^2 = \sum_{j\in(x,y,z)} &\left(\frac{\partial^2 T_j}{\partial x^2}(\mathbf{r})\right)^2 + \left(\frac{\partial^2 T_j}{\partial y^2}(\mathbf{r})\right)^2 \\ &+ \left(\frac{\partial^2 T_j}{\partial z^2}(\mathbf{r})\right)^2 + 2\left(\frac{\partial^2 T_j}{\partial x\partial y}(\mathbf{r})\right)^2 \\ &+ 2\left(\frac{\partial^2 T_j}{\partial x\partial z}(\mathbf{r})\right)^2 + 2\left(\frac{\partial^2 T_j}{\partial y\partial z}(\mathbf{r})\right)^2\end{aligned} \quad (3)$$

with $\mathbf{T} = [T_x, T_y, T_z]$, n the number of points $\mathbf{r}$, and α a factor to modulate the influence of the smoothness penalty. In every frame, pixels outside the ultrasound sector were masked to ensure that this part of the image did not contribute to the calculations in the registration process.

The current choices for the different components in the registration framework have all been proven to be useful for myocardial motion estimation from ultrasound data (De Craene et al. 2012b; Elen et al. 2008; Ledesma-Carbayo et al. 2005).

In practice, subsequent images in the cardiac cycle were first registered to each other in a pairwise fashion. To find the transformation field $\mathbf{T}$ in frame f with respect to end-diastole (ED), inter-frame transformation fields were cumulated:

$$\mathbf{T}_{\mathrm{ED}\to f}(\mathbf{r}) = \mathbf{T}_{\mathrm{f}-1\to f}(\mathbf{r}) \circ \cdots \circ \mathbf{T}_{2\to 3}(\mathbf{r}) \circ \mathbf{T}_{\mathrm{ED}\to 2}(\mathbf{r}) \quad (4)$$

The method was implemented within the ITK framework, a collection of open-source C++ image analysis libraries (Yoo et al. 2002).

To assess strain within a certain region of interest (ROI), the endo- and epicardial borders were first manually contoured in a number of slices at end-diastole using custom-made software (Speqle3D, KU Leuven, Leuven, Belgium) (see Fig. 2a). A least-squares surface fitting procedure with a fifth-order spherical harmonics expansion was used to generate endo- and epicardial surfaces (Claus et al. 2008), which were subsequently labeled corresponding to a standard 18-segment LV model (Fig. 2b) (Cerqueira et al. 2002). Next, this ROI was populated with a 3-D myocardial mesh of 9000 points, sampled along the directions of a local cardiac coordinate system (5, 30 and 60 samples in the radial, longitudinal and circumferential directions, respectively). Finally, the generated mesh was propagated over the cardiac cycle using the estimated inter-frame transformation fields.

Strain $\varepsilon_{\mathrm{d,\ ED}\to f}$ in every point along a certain cardiac direction d was calculated according to

$$\varepsilon_{\mathrm{d,\ ED}\to f} = \frac{L_{\mathrm{d}}(f) - L_{\mathrm{d}}(\mathrm{ED})}{L_{\mathrm{d}}(\mathrm{ED})} \quad (5)$$

where $L_{\mathrm{d}}(f)$ is the distance between two adjacent sample points in either the radial, longitudinal or circumferential direction at frame f; and $L_{\mathrm{d}}(\mathrm{ED})$ is the respective initial distance at ED. The estimated strain curves were drift compensated to obtain values of zero strain at the end of the cardiac cycle (ED2) by distributing the remaining strain offset $\varepsilon_{\mathrm{d,ED}\to\mathrm{ED2}}$ uniformly over the cardiac cycle (containing N frames). The drift-compensated strain $\varepsilon^{dr}_{\mathrm{d,}}$ $\mathrm{ED}\to f$ in frame f thus becomes

$$\varepsilon^{dr}_{\mathrm{d,\ ED}\to f} = \varepsilon_{\mathrm{d,\ ED}\to f} - \frac{f-1}{N-1}\,\varepsilon_{\mathrm{d,\ ED}\to\mathrm{ED2}} \quad (6)$$

Finally, strain values were averaged within each segment and end-systolic (ES) strain values were extracted in the infero-lateral wall. The end-systolic frame was visually defined based on the timing of aortic valve closure (AVC).

Sonomicrometry

Reference strain curves were obtained by post-processing the recorded crystal traces using custom-made software. Inter-crystal distance could be calculated continuously at a time resolution of 1 ms and with a spatial resolution of 15.4 μm by using the speed-of-sound (1530 m/s) and the time of flight between ultrasound emission and detection in a neighboring crystal. The following steps were performed successively for all traces: data outliers were removed automatically by median filtering, parts of the crystal traces with a low quality (*e.g.,* due to signal loss) could be removed manually if required, the ED of every consecutive cardiac cycle was identified based on the onset of the simultaneously recorded LV pressure and the reference displacements were averaged over different cycles. Similar to the registration method, strain was calculated according to eqn (5). ES values were determined at AVC, defined by $(dP/dt)_{\min}$ − 20 ms (Theroux et al. 1976). To account for any physiological changes occurring during the course of the procedure, reference ES strain values were obtained by averaging recordings made before and after the acquisition of the US data.

Statistical analysis

The calculated 3-D end-systolic strain values were correlated with the reference ES strain values by sonomicrometry using the Pearson correlation coefficient. (p values < 0.05 were considered significant). The

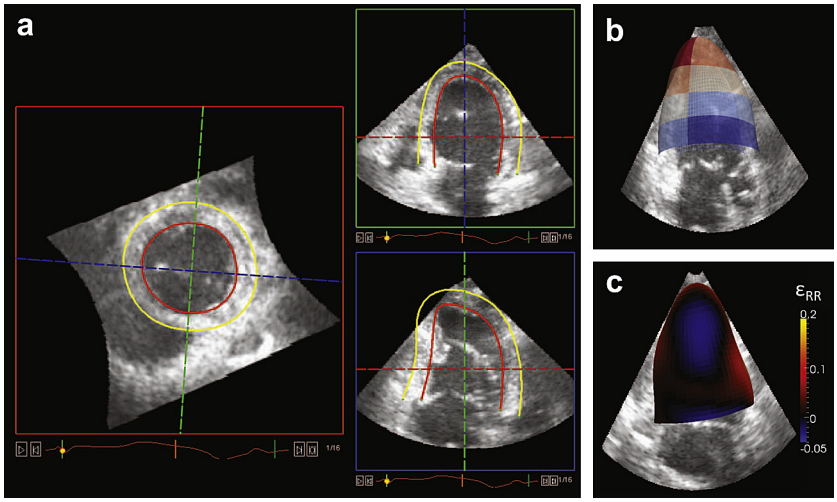

Fig. 2. General workflow to assess 3-D strain: (a) The region of interest is manually delineated using custom-made software (Speqle3D, KU Leuven, Leuven, Belgium) in a select number of image slices. (b) Next, a 3-D myocardial mesh is created using these contours (the colors indicate the 18-segment left ventricle model). (c) Using the image registration results, this mesh is deformed over the cardiac cycle, and strain is calculated (the color overlay shows the end-systolic radial strain in a data set during acute ischemia in the mid infero-lateral wall).

agreement between the two methodologies was evaluated using Bland-Altman analysis of the systolic strain values.

Eight randomly selected data sets (*i.e.,* two data sets during baseline, dobutamine, esmolol and ischemia conditions) were reprocessed using the elastic image registration method for the assessment of 3-D strain reproducibility. Intra-observer variability was expressed as the mean percentage error (absolute difference divided by the mean of the two measurements).

RESULTS

The correlation coefficients between the estimated ES strain and the reference ES strain values were $r = 0.69$ for ε_{RR} ($p < 0.001$), $r = 0.64$ for ε_{LL} ($p < 0.001$) and $r = 0.62$ for ε_{CC} ($p < 0.001$), as shown in Figure 3. Bland-Altman analysis revealed the bias and the 95% limits of agreement for the radial, longitudinal and circumferential component to be $0.02 \pm 13.01\%$, $-1.48 \pm 6.36\%$ and $-4.21 \pm 9.40\%$, respectively (Fig. 4).

Examples of strain curves obtained with the registration method and sonomicrometry are shown in Figure 5 during baseline conditions and acute ischemia. Figure 6 illustrates the strain changes occurring during acute ischemia.

Intra-observer variability was 8.5%, 5.8% and 3.5% for ε_{RR}, ε_{LL} and ε_{CC}, respectively.

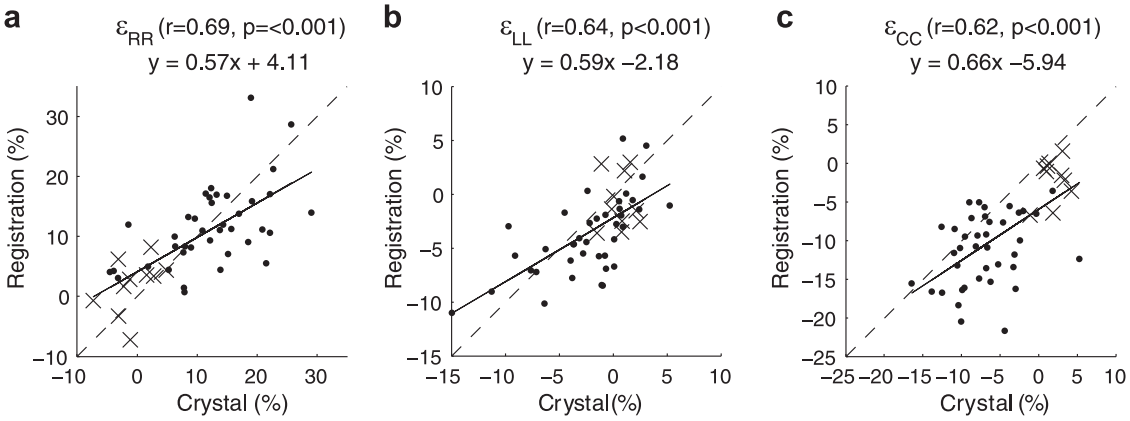

Fig. 3. End-systolic strain estimated by the registration method versus reference end-systolic strain calculated from sonomicrometry in the (a) radial, (b) longitudinal and (c) circumferential directions. Crossed points originate from data sets acquired during acute ischemia. The dashed line represents the line of unity.

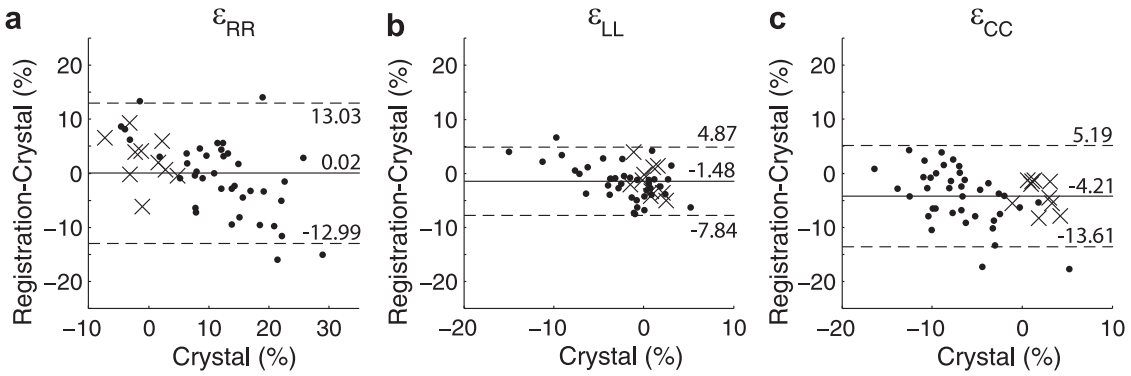

Fig. 4. Bland-Altman plot of end-systolic strain values obtained with the registration method and sonomicrometry in the (a) radial, (b) longitudinal and (c) circumferential directions. Crossed points originate from data sets acquired during acute ischemia. The dashed horizontal lines represent the limits of agreement (mean ± 1.96 SD).

DISCUSSION

Despite the abundance of articles demonstrating regional 3-D strain estimation within a clinic context, only a limited number of studies have validated these 3-D strain algorithms in an *in vivo* experimental setting (see Table 1). This setup is favored over simulated images or phantom experiments as it provides a more realistic motion pattern and image quality is closer to what is seen in clinical practice. The aim of the present study, therefore, was to validate our previously proposed 3-D strain estimation methodology on a segmental level in an animal model for which a ground truth deformation estimate is available.

Significant and encouraging correlations were obtained for all cardiac directions, with slightly higher values in the radial ($r = 0.69$) direction than in the other directions ($r = 0.64$ for ε_{LL}, and $r = 0.62$ for ε_{CC}). Compared with our previous preliminary results (Heyde et al. 2011), radial correlation was much better (from $r = 0.21$ to $r = 0.69$). This is probably due to the increased number of animals (from 5 to 14) and the increased ε_{RR} range as more ischemic data sets were available (originally only three were analyzed).

These findings are in agreement with the current state-of-the-art commercial 3-D speckle tracking methods, which typically rely on block matching-based algorithms. In a study by Seo et al. (2009), regional correlations of $r = 0.59$–0.70 for ε_{RR}, $r = 0.65$–0.68 for ε_{LL} and $r = 0.71$–0.78 for ε_{CC} were obtained against microcrystals in an animal population of 10 sheep.

A comparable registration method developed by Myronenko et al. (2009) gave high correlations ($r = 0.88$–0.93) against sonomicrometry traces. It is important to note that strain values were calculated between crystal pairs that were spread out over multiple segments, and that were not necessarily aligned to the cardiac directions. In contrast, in the present study all crystal pairs were located within one segment and oriented along the cardiac directions.

The correlations found in this study are also consistent with our previous *in vivo* study in which we assessed the performance of this registration method on 2-D images in a subgroup of these animals (Heyde et al. 2013). Radial strain had the highest correlation ($r = 0.85$), closely followed by correlations in the other directions ($r = 0.7$ for ε_{LL}, and $r = 0.73$ for ε_{CC}).

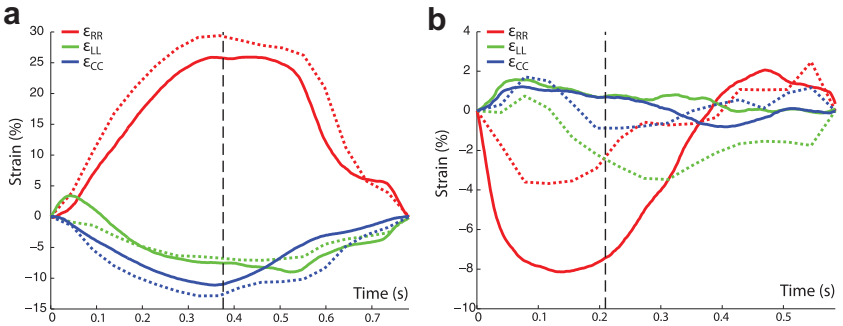

Fig. 5. Estimated strain values (dotted line) versus reference strain values (solid line) for (a) data set at baseline conditions and (b) during acute ischemia.

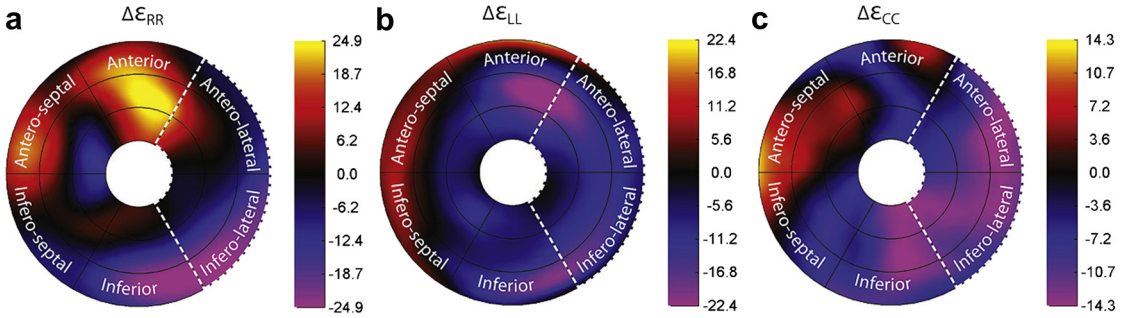

Fig. 6. Bull's-eye plot illustrating the spatial distribution of the change in end-systolic (a) radial, (b) longitudinal and (c) circumferential strain during acute ischemia of the left circumflex artery (LCX) compared with baseline conditions ($\Delta\varepsilon = |\varepsilon_{ischemia}| - |\varepsilon_{baseline}|$). The typical LCX perfusion area is represented by a dashed line (Ortiz-Pérez et al. 2008).

As can be seen from the Bland-Altman plots (Fig. 4), the method seemed to overestimate excursions specifically in the circumferential direction (−4.21%), while bias in the longitudinal direction was lower (−1.48%), and even negligible for the radial direction (0.02%). Nevertheless, the limits of agreement (LOA) were largest for the radial component, whereas the smallest variability was seen for ε_{LL}. The observed ε_{CC} bias may be explained by the fact that circumferential strain was averaged over the myocardial wall while the crystal pair was placed epicardially. Indeed, it is well known that a heterogeneous transmural strain distribution exists with the lowest circumferential strain located at the epicardium (Bogaert and Rademaekers 2001). The large variability in the radial direction could be related to the fact that the spatial motion gradient has to be estimated within a relatively small region because of the limited wall thickness. Furthermore, because the left ventricle is typically scanned from an apical view in 3-D echocardiography, beam density and, consecutively, spatial resolution are lower in the radial direction than in the longitudinal direction. It is also worth mentioning that even with 2-D strain estimation techniques, radial strain estimation has been more difficult and prone to errors (Langeland et al. 2006).

Comparing the observed LOA with the literature is difficult, as no other studies have reported this on a segmental level. In the study by Seo et al. (2009) using a block matching-based approach, Bland-Altman plots were only made for all segments simultaneously. Nevertheless, the LOA were narrower in all directions for our registration method (Table 1: 13% vs. 14%; 6% vs. 10%; and 9% vs. 13% for ε_{RR}, ε_{LL} and ε_{CC}, respectively). These findings may be explained in terms of the underlying tracking mechanism which differs for the two techniques. Block matching-based methods rely on tracking local stable speckle patterns using correlation criteria, whereas registration methods use a more global approach in which the entire cardiac motion field is estimated by optimizing a similarity criterion between subsequent frames. As such, regularization is intrinsically embedded in the registration-based techniques (e.g., the recovered motion field should be smooth), whereas block matching methods typically require *an a posteriori* regularization step *(e.g.*, discarding motion estimates that have a low tracking quality followed by median filtering). In addition to tracking local features (speckles), registration methods also take global features into account (*e.g.*, strong endocardial and epicardial borders). Registration methods may therefore retrieve motion better when large displacements occur, as the associated decorrelation of the speckle pattern may lead to undesirable results for the speckle tracking method.

Intra-observer variability was remarkably lower for our registration method compared with the reproducibility reported by Seo et al. (2009): 8.5% versus 13.5% for ε_{RR}, 5.8% versus 7.8% for ε_{LL} and 3.5% versus 8.9% for ε_{CC}, respectively. This may be related to the fact that the registration method produces a dense motion field for the complete image irrespective of the chosen ROI, whereas the block matching-based method typically estimates motion in a predefined ROI only. Reanalyzing the data with a slightly different ROI may thus result in a different selection of stable speckle patterns, which may lead to higher intra-observer variability.

Finally, Figure 6 illustrates that the registration method is also able to detect deformation changes occurring in the perfusion area of a coronary artery during an acute occlusion. Indeed, as can be noted from Figure 6a, end-systolic ε_{RR} dropped considerably in the left circumflex perfusion area. Similarly, both ε_{LL} and ε_{CC} estimates decreased (*i.e.,* became less negative) during artery occlusion. This corresponds to the expected strain behavior during ischemic phases (Bijnens et al. 2007).

Table 1. Overview of different experimental validation studies in echocardiography to quantify regional myocardial deformation*

Approach	Validation study	Number†	Segments‡	ε_{RR}	ε_{LL}	ε_{CC}	ε_{acr}§	ε_{pp}¶
Block matching	Duan et al. (2009)#	3	Single	—	—	—	—	0.83–0.91 (1.8 ± 3.56%)
	Seo et al. (2009)	10	Multiple	0.84 (3 ± 14%)	0.89 (2 ± 10%)	0.9 (−3 ± 13%)	—	—
			Separately	0.59–0.7	0.65–0.68	0.71–0.78	–	—
	Seo et al. (2011)	8	Multiple	—	—	—	0.87 (0.45 ± 17.8%)	—
Registration	Myronenko et al. (2009)#	5	Multiple	—	—	—	—	0.88–0.93
	Heyde et al. (2011)#	5	Single	0.21‖	0.63	0.60	—	—
	Present paper	14	Single	0.69 (0.02 ± 13.01%)	0.64 (−1.48 ± 6.36%)	0.62 (−4.21 ± 9.40%)	—	—
Model-based	Papademetris et al. (2001)	4	Multiple	—	—	—	—	0.89

* Methods were classified according to Jasaityte et al. (2013). Correlation coefficients (r) against sonomicrometry are reported. Values in parentheses are the limits of agreement expressed as the mean bias ± 1.96 SD, if reported in the associated study.
† Number of animals in the validation study.
‡ Some validation studies used multiple crystal pairs placed in different segments to assess a particular strain component. Correlations can therefore be reported using *multiple* segments together or for every segment *separately* leading to a range of correlation values. In all other cases, only one crystal pair for each strain component was available and the correlation was reported in a *single* segment.
§ Area change ratio (as a substitute for ε_{RR}).
¶ Principal strain (average of all three principal strain components).
‖ Not significant ($p = 0.42$).
Proceedings paper presented at a conference.

Limitations

In the present study only strain values within the inferolateral wall were assessed as this was the only segment in which reference values were available. Although in theory more crystal pairs could be implanted, the amount of crystals that could be acquired simultaneously was limited by the sonomicrometry system (in our case, a maximum of seven crystals). Moreover, it would have also prolonged an already complex experimental protocol.

Aligning US acquisitions and crystal traces in time is challenging given that both acquisition systems interfere and, thus, cannot operate simultaneously. In the present study, aortic valve closure was visually identified on the echocardiographic recordings to define end-systole in the ultrasound sequence. On the other hand, for the crystal data, AVC was selected based on simultaneously recorded LV pressures using a previously validated methodology (taking $(dP/dt)_{min} - 20$ ms) (Theroux et al. 1976). These different approaches to the definition of end-systole may have induced small timing errors with corresponding errors for the end-systolic strain values.

To improve this temporal registration process in future experiments, it may be better to continuously record pressure data. In this way, the ultrasound images could be temporally aligned with the pressure data by cross-correlation of the electrocardiographic signals recorded simultaneously by both acquisition systems (*i.e.,* the ultrasound scanner and the physiologic data acquisition system). As such, AVC could always be defined on the pressure traces and then imposed on the (time-registered) ultrasound images and the sonomicrometry signals (intrinsically time aligned, as these signals are sampled by the same physiologic data acquisition system). Of course, this approach would imply that the physiology of the animal does not change between the ultrasound and sonomicrometry recordings, which is a reasonable assumption given the recordings are made immediately after one another. In the current study, this timing approach could not be used given that the entire physiologic data acquisition system, rather than the sonomicrometry system alone, was switched off during ultrasound recordings.

Whether 3-D elastic registration performs better than 3-D block matching-based methodologies still remains to be proven. Nevertheless, as 3-D ultrasound typically comes at the expense of temporal resolution with associated de-correlation between subsequent volumes, elastic registration may be more robust as it uses a more global motion estimation approach.

Also worth noting is that in general, motion estimation approaches rely on good image quality. Because volumetric data were acquired through a sternotomy,

only two data sets had to be excluded from analysis. In clinical practice, however, the quality of the volumetric images may be inferior (feasibility ranges from 63% to 83%) (Jasaityte et al. 2013) and may thus affect tracking quality. Indeed, clinically 3-D strain values have been compared with 2-D techniques, for example, by Maffessanti et al. (2009), who found only moderate segmental correlations of $r = 0.49$ and $r = 0.43$ for ε_{LL} and ε_{CC}, respectively, whereas radial correlation was poor ($r = 0.24$). These observations are consistent with a previous clinical study in which we compared the 3-D segmental strain estimates against those obtained with 2-D techniques ($r = 0.63$ for ε_{LL}, $r = 0.41$ for ε_{CC} and no significant correlation for ε_{RR}) (Jasaityte et al. 2012).

Future perspectives

Despite the great potential of 3-D echocardiography to quantify regional cardiac function, some emerging shortcomings may potentially hamper widespread use in clinical practice in the future. First, a recent study demonstrated that the inter-vendor variability of commercially available software packages in assessing 3-D strain was high (Gayat et al. 2011). Apart from using different underlying tracking algorithms, this may also be due to a lack of standardization (*e.g.,* Should peak or ES strain be reported? How is ED defined? Should strain be measured in the sub- or mid-myocardium?) It is worth mentioning that a working group of experts has recently been formed by the European Association of Cardiovascular Imaging and the American Society of Echocardiography to work on the standardization of 2-D strain estimation software. Extending the focus to 3-D strain estimation would thus be beneficial.

Furthermore, validation and comparison of different 3-D strain methodologies have been difficult because of a lack of benchmark data. Very recently, De Craene et al. (2012a) initiated the construction of publicly available 3-D benchmark data. Currently, the database consists of simulated data covering healthy, ischemic and left bundle branch block images. The validation protocol presented in this article may inspire further extension of the database to include more realistic images.

CONCLUSIONS

In this study, we found that all strain components could be estimated with acceptable accuracy from volumetric ultrasound data sets in an animal model. These findings are comparable to the performance of the current state-of-the-art commercial 3-D speckle tracking methods. Furthermore, the shape of the strain curves, the timing of peak values and the location of dysfunctional regions were identified well. Whether 3-D elastic registration performs better than 3-D block matching-based methodologies still remains to be proven.

Acknowledgments—The present work was partly funded by the Research Foundation-Flanders (Belgium, FWO-Vlaanderen) under grant G.0693.09. The authors would like to thank J. Vandenweghe and F. Ingelberts from GE Belgium for providing the ultrasound system, and Siemens Ultrasound (Mountain View, CA, US) for their financial contribution to this project.

REFERENCES

Bijnens B, Claus P, Weidemann F, Strotmann J, Sutherland G. Investigating cardiac function using motion and deformation analysis in the setting of a coronary artery disease. Circulation 2007;116: 2453–2464.

Bogaert J, Rademaekers F. Regional nonuniformity of normal adult human left ventricle. Am J Physiol Heart Circ Physiol 2001;280: H610–H620.

Byrd R, Lu P, Nocedal J, Zhu C. A limited memory algorithm for bound constrained optimization. SIAM J Sci Comput 1995;16:1190–1208.

Cerqueira M, Weissman N, Dilsizian V, Jacobs A, Kaul S, Laskey W, Pennell D, Rumberger J, Ryan T, Mario V. Standardized myocardial segmentation and nomenclature for tomographic imaging of the heart. Circulation 2002;105:539–542.

Claus P, Choi H, D'hooge J, Rademakers F. On the calculation of principle curvatures of the left-ventricular surfaces. In: IEEE Engineering in Medicine and Biology Society Conference, 2008. pp. 961–964.

Crosby J, Amundsen B, Hergum T, Remme E, Langeland S, Torp H. 3-D speckle tracking for assessment of regional left ventricular function. Ultrasound Med Biol 2009;35:458–471.

De Craene M, Allain P, Gao H, Prakosa A, Marchesseau S, Somphone O, Hilpert L, Manrique A, Delingette H, Makram-Ebeid S, Villain N, D'hooge J, Sermesant M, Saloux E. Computational and physical phantom setups for the second cardiac motion analysis challenge (cMAC2). In: Camara O, Mansi T, Pop M, Rhode K, Sermesant M, Young A, (eds). Statistical atlases and computational models of the heart: Imaging and modeling challenges. Lecture Notes in Computer Science, Vol. 7746. New York: Springer; 2012a. p. 125–133.

De Craene M, Piella G, Camara O, Duchateau N, Silva E, Doltra A, D'hooge J, Brugada J, Sitges M, Frangi A. Temporal diffeomorphic free-form deformation: Application to motion and strain estimation from 3D echocardiography. Med Image Anal 2012b;16:427–450.

Duan Q, Angelini E, Herz S, Ingrassia C, Costa K, Holmes J, Homma S, Laine A. Region-based endocardium tracking on real-time three-dimensional ultrasound. Ultrasound Med Biol 2009;35:256–265.

Elen A, Choi H, Loeckx D, Gao H, Claus P, Suetens P, Maes F, D'hooge J. 3D cardiac strain estimation using spatio-temporal elastic registration of ultrasound images: A feasibility study. IEEE Trans Med Imaging 2008;27:1580–1591.

Gayat E, Ahmad H, Weinert L, Lang R, Mor-Avi V. Reproducibility and inter-vendor variability of left ventricular deformation measurements by three-dimensional speckle-tracking echocardiography. J Am Soc Echocardiogr 2011;24:878–885.

Heyde B, Cygan S, Choi H, Lesniak-Plewinska B, Barbosa D, Elen A, Claus P, Loeckx D, Kaluzynski K, D'hooge J. Regional cardiac motion and strain estimation in three-dimensional echocardiography: A validation study in thick-walled univentricular phantoms. IEEE Trans Ultrason Freq Control 2012;59:668–682.

Heyde B, Jasaityte R, Barbosa D, Robesyn V, Bouchez S, Wouters P, Maes F, Claus P, D'hooge J. Elastic image registration versus speckle tracking for 2D myocardial motion estimation: A direct comparison in vivo. IEEE Trans Med Imaging 2013;32:449–459.

Heyde B, Jasaityte R, Bouchez S, Vandenheuvel M, Loeckx D, Claus P, Wouters P, D'hooge J. Three-dimensional myocardial strain estimation from volumetric ultrasound: Experimental validation in an animal model. In: IEEE International Ultrasonics Symposium, Orlando, FL, USA, 2011:1862–1865.

Jasaityte R, Heyde B, D'hooge J. Current state of three-dimensional myocardial strain estimation using echocardiography. J Am Soc Echocardiogr 2013;26:15–28.

Jasaityte R, Heyde B, Ferferieva V, Amundsen B, Barbosa D, Loeckx D, Kiss G, Orderud F, Claus P, Torp H, D'hooge J. Comparison of a new methodology for the assessment of 3D myocardial strain from volumetric ultrasound with 2D speckle tracking. Int J Cardiovascular Imaging 2012;28:1049–1060.

Kukulski T, Jamal F, Herbots L, D'hooge J, Bijnens B, Hatle L, De Scheerder I, Sutherland G. Identification of acutely ischemic myocardium using ultrasonic strain measurements. J Am Coll Cardiol 2003;41:810–819.

Kybic J, Unser M. Fast parametric elastic image registration. IEEE Trans Image Process 2003;12:1427–1442.

Langeland S, Wouters P, Claus P, Leather A, Bijnens B, Sutherland G, Rademakers F, D'hooge J. Experimental assessment of a new research tool for the estimation of two-dimensional myocardial strain. Ultrasound Med Biol 2006;32:1509–1513.

Ledesma-Carbayo M, Kybic J, Desco M, Santos A, Suhling M, Hunziker P, Unser M. Spatio-temporal nonrigid registration for ultrasound cardiac motion estimation. IEEE Trans Med Imaging 2005;24:1113–1126.

Leung E, Danilouchkine M, van Stralen M, de Jong N, van der Steen A, Bosch J. Left ventricular border tracking using cardiac motion models and optical flow. Ultrasound Med Biol 2011;37:605–616.

Lopata R, Nillesen M, Thijssen J, Kapusta L, de Korte C. Three-dimensional cardiac strain imaging in healthy children using RF-data. Ultrasound Med Biol 2011;37:1399–1408.

Maffessanti F, Nesser H, Weinert L, Steringer-Mascherbauer R, Niel J, Gorissen W, Sugeng L, Lang R, Mor-Avi V. Quantitative evaluation of regional left ventricular function using three-dimensional speckle tracking echocardiography in patients with and without heart disease. Am J Cardiol 2009;104:1755–1762.

Marwick T. Will standardization make strain a standard measurement? J Am Soc Echocardiogr 2012;25:1204–1206.

Mor-Avi V, Lang R, Badano L, Belohlavek M, Cardim N, Derumeaux G, Galderisi M, Marwick T, Nagueh S, Sengupta P, Sicari R, Smiseth O, Smulevitz B, Takeuchi M, Thomas J, Vannan M, Voigt J, Zamorano J. Current and evolving echocardiographic techniques for the quantitative evaluation of cardiac mechanics: ASE/EAE consensus statement of methodology and indications. J Am Soc Echocardiogr 2011;24:277–313.

Myronenko A, Song X, Sahn D. Maximum likelihood motion estimation in 3D echocardiography through non-rigid registration in spherical coordinates. In: Functional Imaging and Modeling of the Heart. Lecture Notes in Computer Science, Vol. 5528. New York: Springer; 2009. p. 427–436.

Ortiz-Pérez J, Rodríguez J, Meyers S, Lee D, Davidson C, Wu E. Correspondence between the 17-segment model and coronary arterial anatomy using contrast-enhanced cardiac magnetic resonance imaging. JACC Cardiovascular Imaging 2008;1:282–293.

Papademetris X, Sinusas A, Dione D, Duncan J. Estimation of 3D left ventricular deformation from echocardiography. Med Image Anal 2001;5:17–28.

Reant P, Barbot L, Touche C, Dijos M, Arsac F, Pillois X, Landelle M, Roudaut R, Lafitte S. Evaluation of global left ventricular systolic function using three-dimensional echocardiography speckle tracking strain parameters. J Am Soc Echocardiogr 2012;25:68–79.

Rueckert D, Sonoda L, Hill D, Leach M, Hawkes D. Nonrigid registration using free-form deformations: Application to breast MR images. IEEE Trans Med Imaging 1999;18:712–721.

Seo Y, Ishizu T, Enomoto Y, Sugimori H, Aonuma K. Endocardial surface tracking for assessment of regional LV wall deformation with 3D speckle tracking imaging. J Am Coll Cardiol 2011;4: 358–365.

Seo Y, Ishizu T, Enomoto Y, Sugimori H, Yamamoto M, Machino T, Kawamura R, Aonuma K. Validation of 3-dimensional speckle tracking imaging to quantify regional myocardial deformation. Circ Cardiovasc Imaging 2009;2:451–459.

Somphone O, Makram-Ebeid S, Cohen L. Robust image registration based on a partition of unity finite element method. In: International Symposium on Biomedical Imaging, 2008:1123–1126.

Theroux P, Ross J, Franklin D, Kemper W, Sasyama S. Regional myocardial function in the conscious dog during acute coronary occlusion and responses to morphine, propranolol, nitroglycerin, and lidocaine. Circ Res 1976;53:302–314.

Yang L, Georgescu B, Zheng Y, Wang Y, Meer P, Comaniciu D. Prediction based collaborative trackers (PCT): A robust and accurate approach toward 3D medical object tracking. IEEE Trans Med Imaging 2011;30:1921–1932.

Yoo T, Ackerman M, W L, Schroeder W, Chalana V, Aylward S, D M, Whitaker R. Engineering and algorithm design for an image processing API: A technical report on ITK—The Insight Toolkit. In: Studies in Health Technology and Informatics, Proceedings of Medicine Meets Virtual Reality, Vol. 85. Amsterdam: IOS Press, 2002:586–592.

Zitova B, Flusser J. Image registration methods: A survey. Image Vision Comput 2003;21:977–1000.